PROCEEDINGS, 50th Workshop on Geothermal Reservoir Engineering
Stanford University, Stanford, California, February 10-12, 2025
SGP-TR-229

Influence of Hydraulic Fractures on Induced Seismicity: A Case Study of the Pohang Mw 5.5 Earthquake

Yuan Tian and Roland N. Horne

Stanford Geothermal Program, Stanford, California 94305, United States

ytian96@stanford.edu

Keywords: Hydraulic fracture; Induced seismicity; Enhanced Geothermal Systems

ABSTRACT

Identifying the mechanisms of induced seismicity in Enhanced Geothermal Systems (EGS) remains a challenge. In this paper, we propose a multimechanism approach to explain the induced seismicity sequence of the 2017 Mw 5.5 earthquake in the Pohang Enhanced Geothermal System, based on on-site seismicity data. We investigated two mechanisms, fluid pressure and tensile stress transfer from hydraulic opening, and examined their contributions to distinct stages of the seismicity sequence using a combined flow and geomechanical model. We suggest that tensile stress transfer was activated instantaneously when the hydraulic fractures opened during injection, contributing to the moderate Mw 1.67 event around the time injection stopped. At this point, fluid pressure had not yet reached the fault due to its finite propagation speed and the fault remained inactive. After injection stopped, fracture closure led to the deactivation of both stress and pressure mechanisms, potentially explaining the seismically dormant period observed post-injection. When the pressure front eventually reached the fault, continuous pressure increases led to resumed seismicity. The pressure buildup combined with the delayed arrival of the pressure front may have triggered the Mw 5.5 earthquake which occurred 58 days after injection stopped.

1. INTRODUCTION

Induced seismicity in Enhanced Geothermal Systems (EGS) has received much attention due to large earthquakes occurring during stimulation. These include the Mw 2.94 event in Basel (Haring et al. 2008), and Mw 5.5 in Pohang (Ellsworth et al. 2019), all of which led to the early termination of their respective projects. In EGS, the combination of sensitive geological conditions and high injection pressure can elevate seismicity risk. EGS projects typically target deep crystalline basement formations at depths of 3-5km to reach high temperatures (Kivi et al. 2023), where faults may be well developed and are large enough to host significant earthquake events. Besides, injection pressure is usually high which can exceed the minimal principal stress to enhance permeability of the reservoir.

One key challenge in managing induced seismicity in EGS is the timing of seismic events. Although moderate earthquake events often occur during the injection, large-delayed earthquake have occurred hours to months after injection has stopped, examples include a 5-hour delay in Basel, 1-day delay in Soulz, and 58-day in Pohang. This unpredictability in timing complicates operational design and mitigation strategies, highlighting the need for a better understanding of the mechanisms driving these seismic events and the conditions under which they are activated. Therefore, there is a need to better understand the mechanisms of these seismic events and conditions under which they are activated.

Several mechanisms can perturb fault stress and induce seismicity, each associated with distinct physical processes. The most well-known mechanism is fluid pressure (Ellsworth et al. 2019). When an injection well is hydraulically connected to a fault through rock matrix or fractures, fluid pressure propagates towards the fault by pressure diffusion. Once the pressure front reaches the fault, it decreases the effective normal stress on fault and can induce seismicity. The other mechanism which can perturb stress on fault is stress changes resulting from deformation of the surrounding rock mass or fractures. Subsurface rock is a continuous medium with embedded faults and fractures, where deformation in one area induces stress perturbation elsewhere due to elastic effects. These effects are long-range and activate instantaneously. Poroelasticity is another effect (Segall and Lu 2015, Boyet et al. 2023), in which fluid flow through the porous rock matrix inducing deformation and generating poroelastic stress throughout the rock. Other mechanisms include deformation of faults and fractures, such as slippage of fractures in in hydroshear (Kim et al. 2022), earthquakes on a nearby fault (Catalli et al. 2016) and tensile stress transfer from hydraulic fracture opening (Kettlety et al. 2019). However, the relative contribution of these mechanisms to the induced seismicity sequence in Pohang have not been thoroughly investigated.

The Pohang project initiated in 2011 and was South Korea's first Enhanced Geothermal Systems (EGS) pilot project (Kim et al. 2022). Two boreholes, PX-1 and PX-2, were drilled to depths exceeding 4km (Ellsworth et al. 2019, Woo et al. 2019, KGC 2019). PX-1 was identified as a hydroshear-fracture dominated well, while PX-2 was identified as a hydraulic-fracture dominated well because the maximum well pressure exceeded the minimum principal stress by approximately 26 MPa (Min et al. 2023). Multiple stimulations were conducted in both wells with total injection volume of 5663 m^3 in PX1 and 7136 m^3 in PX2. Following the last (third) stimulation in PX-2, a delayed Mw 5.5 earthquake occurred 58 days after injection stopped (Min et al. 2023). A fault structure was identified based on seismic event locations associated with injection in PX-2 (Woo et al. 2019). During each of the three stimulations, moderate seismic events were observed around the time when injection stopped, with magnitudes of Mw 1.62, Mw 3.2, and Mw 1.67 for the first, second, and third stimulations, respectively. Notably, during the last stimulation, a moderate earthquake (Mw 1.67) occurred at the end of injection, followed by a 58-day seismically dormant period before the large Mw 5.5 earthquake (Min et al. 2023).

There have been several studies on the delayed Mw 5.5 earthquake in Pohang. Chang et al. (2020), Alcolea (2024), Lim et al. (2020) and Yeo et al. (2020) investigated the role of heterogeneous hydraulic diffusivity in the fault zone connecting the well and the fault, which consists of a low diffusivity fault core near the fault and a high diffusivity damage zone. These studies attributed the delayed Mw 5.5 earthquake to the slow pressure diffusion in the fault core and the coupled poroelastic effect. Additionally, Yeo et al. (2020) also considered the role of Coulomb static stress transfer from the Mw 3.0 event during the second stimulation. Kim et al. (2024) investigated the role of the fracture connecting the well and fault, where pressure-dependent permeability in fractures results in a lower diffusivity region near the fault due to pressure drop. In addition, the contribution of shear stress transfer from prior stimulations in the hydrosheared PX-1 well was also investigated (Kim et al. 2024). However, most studies focused on the delayed final Mw 5.5 earthquake with limited attention given to the preceding sequence before the Mw 5.5 event, including the Mw 1.67 at the end of injection and the subsequent 58-day seismically dormant period.

This study aimed to investigate the mechanisms of the induced seismicity sequence associated with the last stimulation in the PX-2 well which was the closest in time to the Mw 5.5 earthquake. The sequence consists of three stages: Stage I is the injection phase, during which a moderate Mw 1.67 earthquake occurred at the end of injection; Stage II is a 58-day seismically dormant period after injection stopped; and stage III is the delayed large earthquake (Mw 5.5). The study evaluated two key mechanisms: fluid pressure and tensile stress transfer from hydraulic fracture opening, and their role in each of the three stages. Results suggest that tensile stress transfer from hydraulic opening, which was activated instantaneously during injection, dominated stage I and contributed to the moderate Mw 1.67 event. After the injection stopped, fracture closure deactivated tensile stress transfer, while pressure propagation of fluid pressure towards the fault was slowed down due to reduced permeability under pressure drop. The deactivation of both mechanisms likely contributed to the seismically dormant period in Stage II. In stage III, the eventual arrival of the fluid pressure front caused an increase in fluid pressure on the fault and triggered the large Mw 5.5 earthquake.

2. EGS PROJECT IN POHANG, SOUTH KOREA

2.1 Tectonic environment

At the Pohang EGS project, two deep boreholes, PX-1 and PX-2, were drilled for hydraulic stimulation (Figure 1). The PX-1 well reached a true vertical depth of 4215 meters and the PX-2 well was drilled to 4340 meters, with their bottom hole locations approximately 600 meters apart (Woo et al. 2019). The maximum recorded wellhead pressure for PX-2 was 89.2 MPa, which was significantly higher than the 27.7 MPa at PX-1. PX-2 was characterized as a hydraulic fracture-dominated well, whereas PX-1 was dominated by hydroshear fractures (Min et al. 2023). The total injection volumes were 5,663 m³ for PX-1 and 7,136 m³ for PX-2. Seismic events were monitored continuously throughout the stimulation phase, revealing two distinct clusters of seismicity associated with PX-1 and PX-2 (Woo et al. 2019, Min et al. 2023). Events related to stimulation in PX-2 were predominantly aligned along a planar structure, which is also where the Mw 5.5 earthquake occurred as the largest event recorded. The structure was identified as a critically stressed fault after the earthquake happened. In this study, the focus was on the stimulation and seismicity related to the PX-2 well.

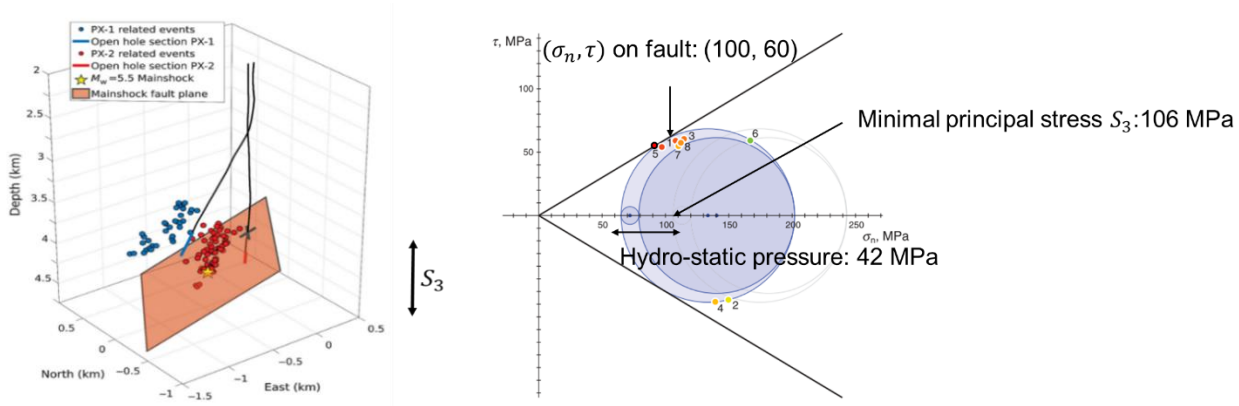

Figure 1: Location of PX-1 and PX-2 wells, the fault, and observed seismicity in Pohang from Woo et al. (2019) (left), in-situ stress conditions in Pohang (right), adapted from Ellsworth et al. (2019).

At the depth of approximately 4.2 km, corresponding to the bottom of the two wells, the in-situ stress state was identified as a reverse fault regime where the minimal principal stress S_3 is in depth direction (Ellsworth et al. 2019). The minimum principal stress was measured at 106 MPa, with hydrostatic pressure approximately as 42 MPa, and its orientation was vertical in depth. The fault was determined to be critically stressed, with an effective normal stress of 90 MPa and a shear stress of 54 MPa.

2.2 Evidence of fractures intersecting PX-2 well

The permeability of the region surrounding the PX-2 well can be inferred from wellhead pressure measurements under constant injection flow rates using the analytical Theis's equation, as shown in (Figure 2). In-situ measurements indicated that permeability increases exponentially with rising wellhead pressure. Specifically, permeability rises from 0.1 mD to 93.6 mD (Park et al. 2017), which is an approximately 1000-fold increase as the wellhead pressure increases from 22 MPa to 89 MPa. This permeability is significantly higher than that of the intact basement rock, which is 7.7×10^{-4} mD (Yeo et al. 2020), suggesting that fractures around the PX-2 well

were likely stimulated. These fractures have much higher hydraulic diffusivity than the surrounding matrix and may become the dominant flow pathways.

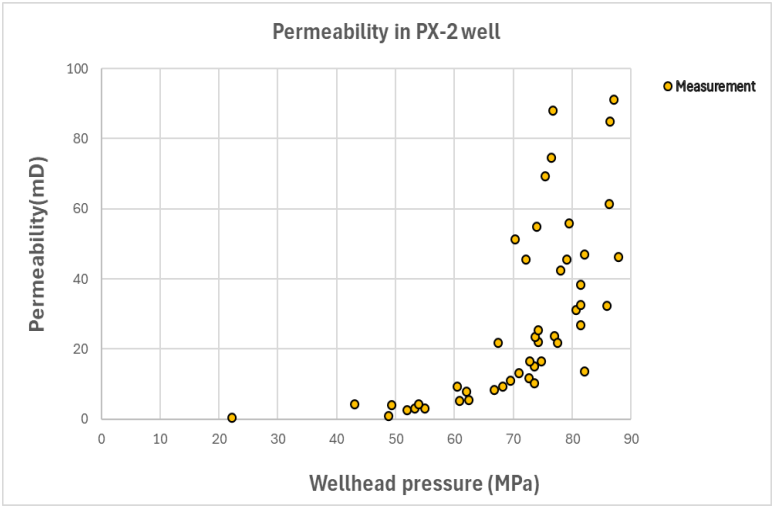

Figure 2: Inferred permeability change with wellhead pressure during the injection test in PX-2 well, adapted from Park et al. (2017).

2.3 Injection and seismicity history in PX-2 well

There have been three stimulations in the PX-2 well with injection volumes of 1970 m^3 for the first, 2831 m^3 for the second, and 2335 m^3 for the third (Figure 3) (Min et al. 2023). Moderate earthquakes were observed at the end of each stimulation, with moment magnitudes of Mw 1.62, Mw 3.2, and Mw 1.67 for the first, second, and third stimulations, respectively. After the seismicity event (Mw 1.67) at the end of the third stimulation, the large Mw 5.5 earthquake occurred with a delay of 58 days.

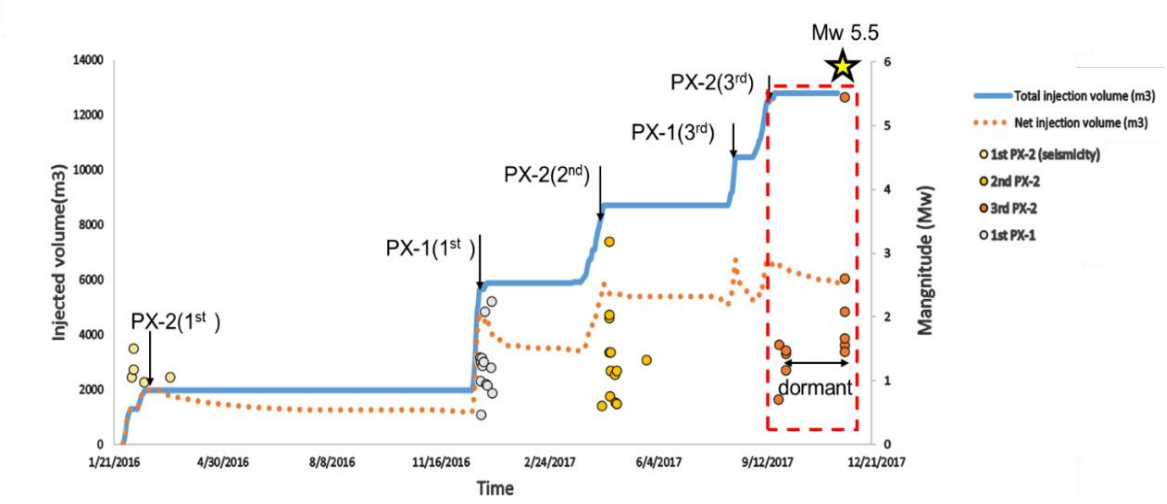

Figure 3: Injection history and observed seismicity history in Pohang adapted from Kim et al. (2022).

2.3 Induced seismicity sequence related to the third stimulation of PX-2 well

This work focused on the induced seismicity sequence related to the last stimulation which was the closest in time to the Mw 5.5 earthquake. As shown in Figure 4, the sequence consisted of three stages: Stage I was the injection phase, during which a moderate Mw 1.67 earthquake occurred at the end of injection; Stage II was a 58-day seismically dormant period after injection stopped; and stage III was the delayed large earthquake (Mw 5.5).

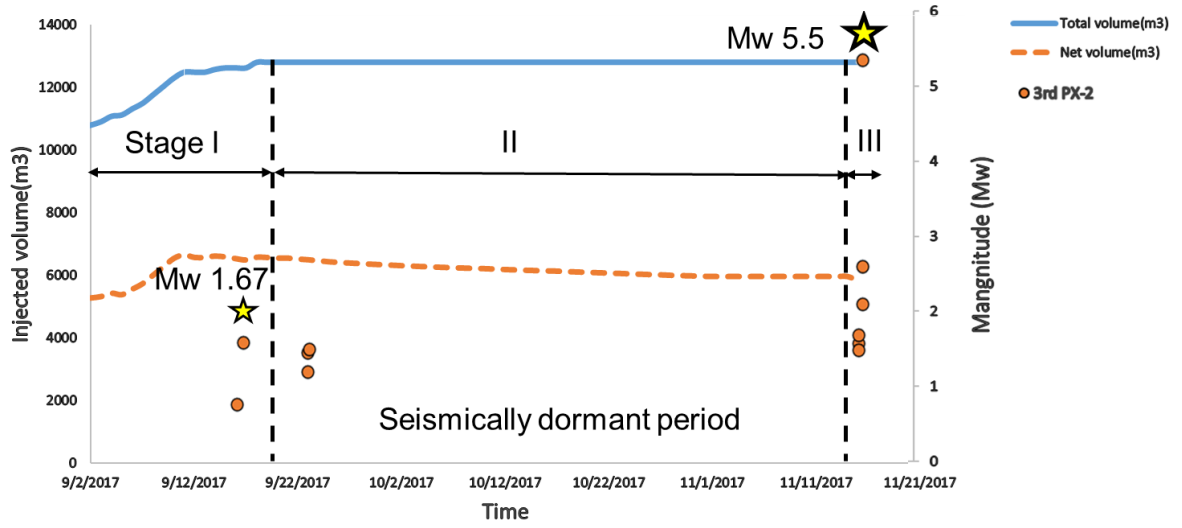

Figure 4: Injection history and seismicity history related to the last stimulation in PX-2 well adapter from Kim et al. (2022).

3. METHODOLOGY

3.1 Conceptual model

This study assumed that a hydraulic fracture plane connects the PX-2 well to the fault hydraulically (Figure 5). Due to its significantly enhanced permeability compared to the surrounding rock, this hydraulic fracture plane is likely to serve as the dominant flow pathway. This assumption is supported by permeability values inferred from the in-situ measurements at the PX-2 well.

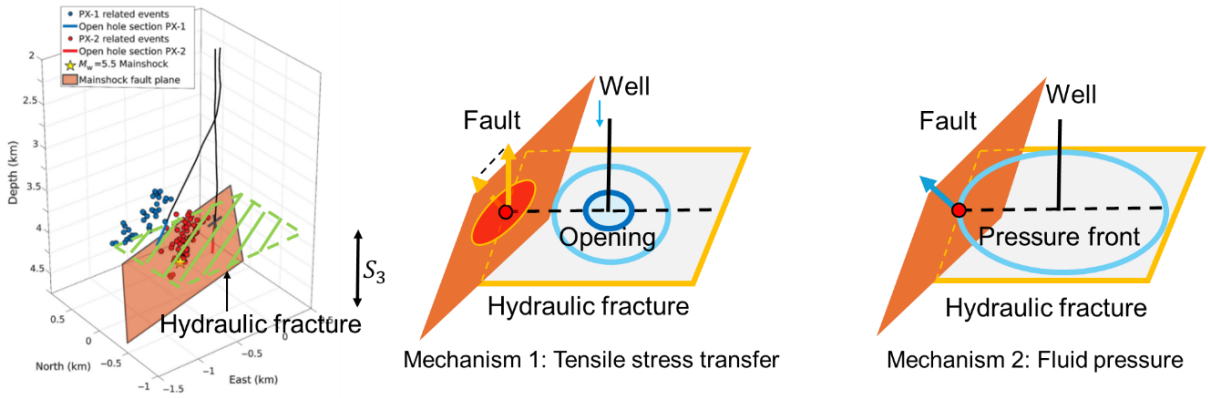

Figure 5: Conceptual model showing a hydraulic fracture can hydraulically connect fault and PX-2 well (left), with two mechanisms for induced seismicity (middle, right).

Two primary mechanisms were considered in this study, both of which can perturb the stress on the fault and potentially contribute to the induced seismicity sequence. The first mechanism is fluid pressure, which reduces the effective normal stress on the fault when the pressure front reaches it. The second mechanism is tensile stress transfer, which arises from the opening of hydraulic fractures. Tensile stress transfer occurs instantaneously upon hydraulic opening and alters the stress field throughout the rock as a long-range effect.

These two mechanisms are derived from distinct physical processes and are activated at different times. Tensile stress transfer is immediate during fracture opening, which occurs during injection, whereas fluid pressure propagates more slowly by pressure diffusion. The propagation speed of fluid pressure depends on the hydraulic diffusivity of the rock, creating a time lag between the activation of these two mechanisms. This conceptual model provides a foundation for understanding the contributions of these mechanisms to the three-stage induced seismicity sequence observed in Pohang. These stages include the Mw 1.67 earthquake during injection (Stage I), the subsequent 58-day seismically dormant period (Stage II), and the delayed Mw 5.5 earthquake (Stage III).

3.2 Modelling procedure

In the modeling procedure, three key parts are involved in investigating the contribution of the two mechanisms that can perturb stress on the fault and trigger induced seismicity (Figure 6). The first part is the flow model, which simulates the pressure change in space and time during the injection phase and after injection stops through pressure diffusion. Based on the pressure distribution, segments where the net

pressure (defined as fluid pressure) exceeds the minimum principal stress are identified as opening segments. Given the net pressure, the fracture mechanics model is applied. The evolution of fluid pressure and tensile stress transfer on the fault is then evaluated. These results serve as inputs to the seismicity model, which calculates slip velocity evolution as an indicator of the observed seismicity magnitude.

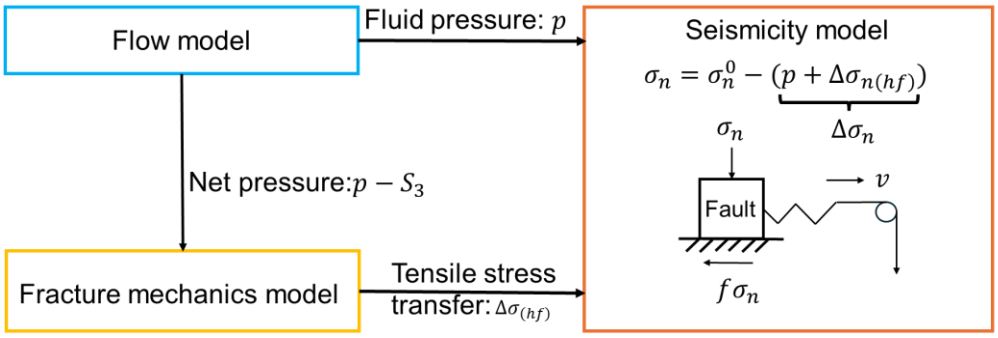

Figure 6: Modelling procedure: flow model, fracture mechanics model and seismicity model.

3.3 Flow model

3.3.1 Governing equation

$$\phi c_t \frac{\partial p}{\partial t} - \left(\frac{\partial q_x}{\partial x} + \frac{\partial q_y}{\partial y}\right) = s, q_x = \frac{k(p)}{\mu}\frac{\partial p}{\partial x}, q_y = \frac{k(p)}{\mu}\frac{\partial p}{\partial y} \quad (1)$$

The governing equation for pressure diffusion in the two-dimensional hydraulic fracture plane intersecting the PX-2 well is given by Equation (1) where ϕ, c_t, q, k, p, μ, s are equivalent porosity, compressibility of fracture, volumetric flux, permeability, pressure, viscosity and source. Additionally, pressure-dependent permeability is used based on in-situ observations. Dividing by ϕc_t on both sides, we obtain Equation (2), where hydraulic diffusivity is introduced as a single input parameter.

$$\frac{\partial p}{\partial t} - \left(\frac{\partial\left(\alpha(p)\frac{\partial p}{\partial x}\right)}{\partial x} + \frac{\partial\left(\alpha(p)\frac{\partial p}{\partial y}\right)}{\partial y}\right) = \frac{s}{\phi c_t}, \qquad \alpha(p) = \frac{k(p)}{\mu\phi c_t} \quad (2)$$

where α is the hydraulic diffusivity. It is assumed that hydraulic diffusivity follows the same exponential increase as permeability. We consider the exponential hydraulic diffusivity pressure relationship to be represented by two parameters as initial hydraulic diffusivity α_0 and enhancement rate d (Rutqvist et al. 1996, Park et al. 2020, Rutqvist et al. 2003).

$$\alpha(p) = \alpha_0 e^{dp} \quad (3)$$

3.3.2 Model setup

A squared mesh was used to simulate radial pressure diffusion in the hydraulic fracture plane using Finite Volume Method. The model size was set to twice the distance between the fault and the injection well, ensuring that the pressure front does not reach the boundary by the end of the simulation (Figure 7). This setup minimizes boundary effect and enables a more accurate pressure solution on fault after the front arrives. Hydraulic diffusivity in the model ranges from 10^{-3} to $10^{0} m^2/s$ with values $\alpha(p = 20MPa) = 1.6 \times 10^{-3} m^2$ and $\alpha(p = 90MPa) = 1.77 m^2$. These values fall within the range of $10^{-4} m^2/s$ to $10 m^2/s$ reported in existing studies in Pohang (Yeo et al., 2020; Chang et al., 2020). Besides, the ratio of hydraulic diffusivity at wellhead pressure 89 MPa to that 22 MPa is 864, and is close to the ratio of inferred permeability, which is 936 in Figure 2. Opening segments are those in which pressure exceeds the minimal principal stress with radius of R_{open}.

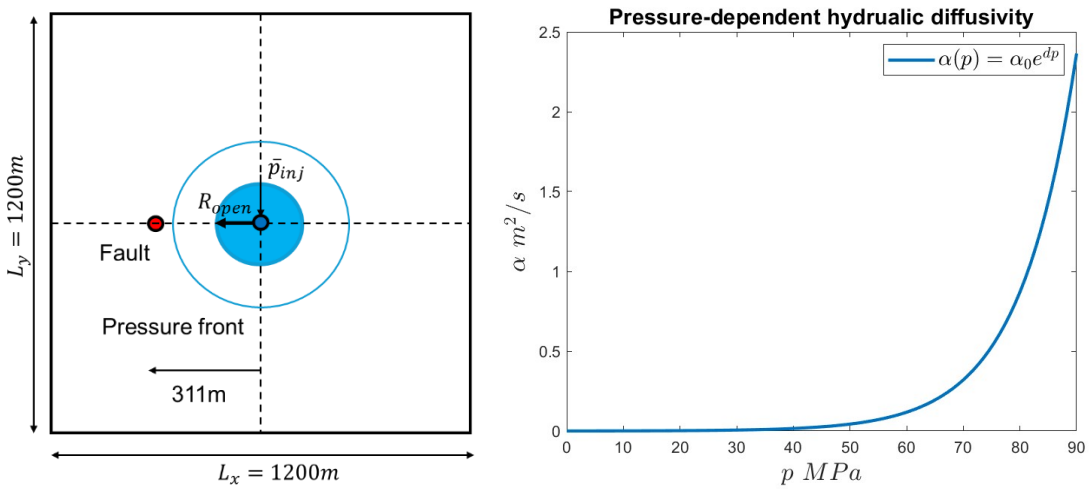

Figure 7: Model geometry for two-dimensional pressure diffusion on the hydraulic fracture plane (left), and the exponential hydraulic diffusivity relationship with pressure (right).

Table 1: Flow model parameters.

Parameter	Value
L_x	1200 m
L_y	1200 m
α_0	2.918 m2/s
d	0.05 MPa-1
$\bar{p}_{inj}$	138 MPa
t_{inj}	93 h
t_{tot}	1551 h

3.3 Fracture mechanics model

3.3.1 Governing equation

$$\begin{cases} \nabla \cdot \boldsymbol{\sigma} = \mathbf{0} \\ \boldsymbol{\sigma} \cdot \boldsymbol{n} = \bar{p}(r) - S_3, r \le R_{open} \ \ (z = 0) \\ [\![u_z]\!] = u_z^+ - u_z^- = 0, \quad r > R_{open} \ \ (z = 0) \end{cases} \Rightarrow \begin{cases} [\![u_z]\!] \ (r \le R_{open}) \\ \Delta\boldsymbol{\sigma} (r > R_{open}) \end{cases} \tag{4}$$

Based on the flow model, segments where the fluid pressure exceeds the minimum principal stress can be identified as opening segments, where the net pressure defined as the difference between fluid pressure and the minimum principal stress is greater than zero. Within the radius of the opening, the fracture mechanics model determines the distribution of the opening size. Beyond the tip of the opening, the associated stress perturbation (Δσ) throughout the surrounding rock, including the fault, can be calculated (Figure 8). This enables the evaluation of the contribution of tensile stress transfer resulting from hydraulic opening.

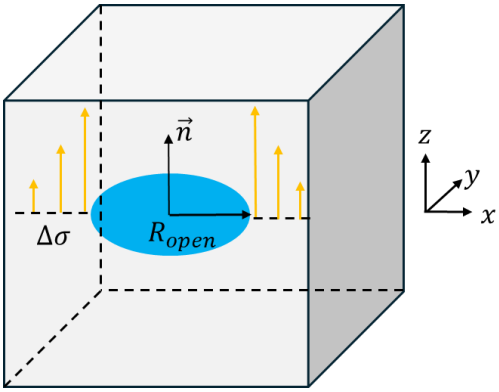

Figure 8: Fracture mechanics model with a two-dimensional hydraulic fracture plane embedded in infinite homogeneous elastic rock.

3.3.2 Model setup and model parameters

A two-dimensional fracture plane with hydraulic opening is embedded in an infinite homogeneous elastic rock with Young's modulus E and Poisson ratio ν. Using the net pressure as input, the Displacement Discontinuity Method (DDM) (Wong et al. 2021) was employed to calculate the distribution of fracture opening and the induced stress field in the surrounding rock beyond the opening.

Table 2: Fracture mechanics parameters.

Parameter	Value
E	40 GPa
ν	0.25

3.4 Seismicity model

When stress on a fault is perturbed, the fault may slip and lead to seismicity, which can be described using a spring-slider model under a quasidynamic approximation (Figure 9). In this model, a friction law is required to relate slip velocity to shear traction. The rate-and-state friction model (Dieterich 1979, Noda et al. 2009, McClure et al. 2011, Ozawa et al. 2023,) is one of the most widely used approaches, effectively capturing the frictional behavior of faults during induced seismicity.

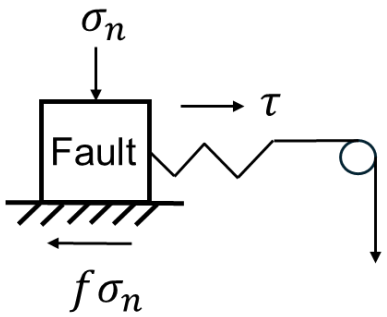

Figure 9: A spring-slider model for seismicity on fault.

3.4.1 Governing equation

The spring-slider model can describe the evolution of slip on fault under perturbed stress:

$$\tau - \eta v = f(v,\theta)\sigma_n \tag{5}$$

$$\sigma_n = \sigma_n^0 - \Delta\sigma_n = \sigma_n^0 - \Delta\sigma_{open} - p \tag{6}$$

where τ, v, σ_n,f, η are shear stress, slip velocity, normal stress, friction coefficient and damping factors. Normal stress on the fault can be perturbed by two key contributions: fluid pressure and tensile stress transfer from hydraulic opening.

The rate-and-state friction model is widely used to describe the friction coefficient for seismicity on a fault. In this model, f_0, v_0, a, b, θ and d_c represent the static friction coefficient, reference velocity, direct effect parameter, evolution effect parameter, state variable, and characteristic slip distance respectively. These parameters collectively define the relationship between friction, slip velocity which can effectively capture the complex frictional behavior of faults during induced seismicity.

$$f(v,\theta) = f_0 + alog\frac{v}{v_0} + blog\frac{\theta}{\theta_0} \tag{7}$$

$$\frac{d\theta}{dt} = 1 - \frac{\theta v}{d_c} \tag{8}$$

3.4.1 Model parameters

Velocity on the fault is evaluated at the intersection point of the hydraulic fracture plane and the fault plane, considering stress perturbations from both fluid pressure and tensile stress transfer induced by hydraulic opening. Equations (8) through (11) are solved using a third-order Runge-Kutta method with adaptive stepping, as detailed in previous studies (Noda et al. 2008, Ozawa et al. 2023).

The slip model parameters are listed in Table 3.

Table 3: Fracture mechanics parameters.

Parameter	Value
f_0	0.6
v_0	1e-6 m/s
a	0.01
b	0.013
d_c	0.0078 m
η	50 MPa·s/m
τ_0	60 MPa
σ_{n0}	99.88 MPa
θ_0	0.6

4. RESULTS AND DISCUSSION

The primary objective of this study was to investigate the mechanisms and associated physical processes responsible for triggering the delayed Mw 5.5 earthquake and the preceding seismicity sequence. This sequence can be categorized into three distinct stages: Stage I corresponds to the injection phase, during which a moderate Mw 1.67 event occurred near when injection stopped. Stage II represents a seismically dormant period with no observed seismicity. Stage III is the occurrence of the Mw 5.5 earthquake. In addition to fluid pressure, tensile stress transfer from hydraulic opening during the stimulation of the PX-2 well is examined as the other contributing mechanism. The roles of these two mechanisms in the three stages of induced seismicity are investigated through flow, fracture mechanics, and seismicity models.

4.1 Stage I: injection

In the model, during Stage I, high-pressure water is injected into the PX-2 well, with the fluid pressure at the bottom of the well exceeding the minimum principal stress and inducing hydraulic opening (Figure 10). Tensile stress is accompanied by the opening, which instantaneously perturbs the stress on the fault once the hydraulic opening forms. In the meantime, fluid pressure propagates towards the fault with a finite speed due to pressure diffusion. In this stage, tensile stress transfer was the dominant mechanism influencing fault stress and is likely responsible for the Mw 1.67 event that occurs near the end of the injection phase. The following sections present the spatial and temporal distributions of fluid pressure and tensile stress transfer during this stage.

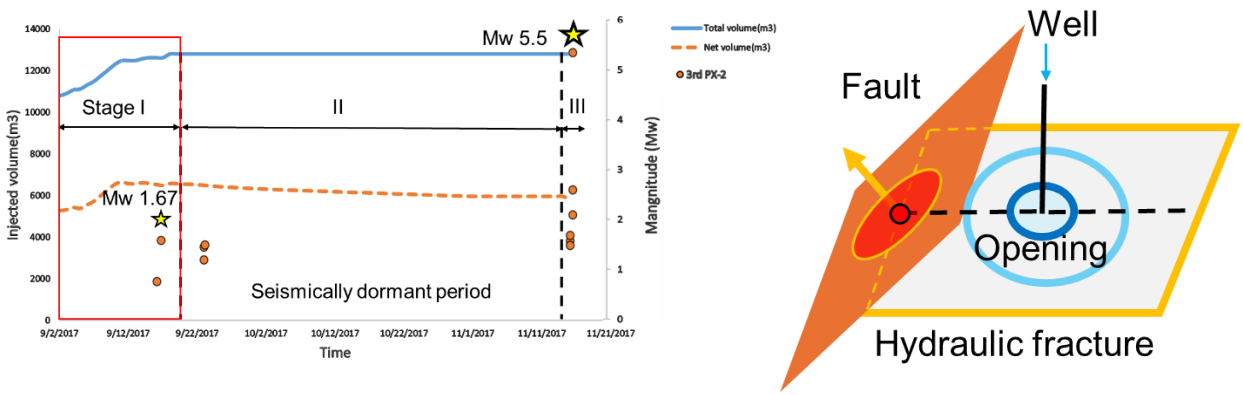

Figure 10: Stage I: injection with Mw 1.67 event in the end(left), dominant mechanism as tensile stress transfer from hydraulic opening (right)

4.1.1 Pressure distribution at the end of injection

During injection, the pressure is highest near the injection point, which is maintained as the 132MPa, and it gradually decreases with distance from the well due to diffusion. At the end of the injection, the fluid pressure front has not reached the fault which is represented as a red circle located 300 meters away from the injection point at (0, 0) and remains hydrostatic pressure (Figure 11).

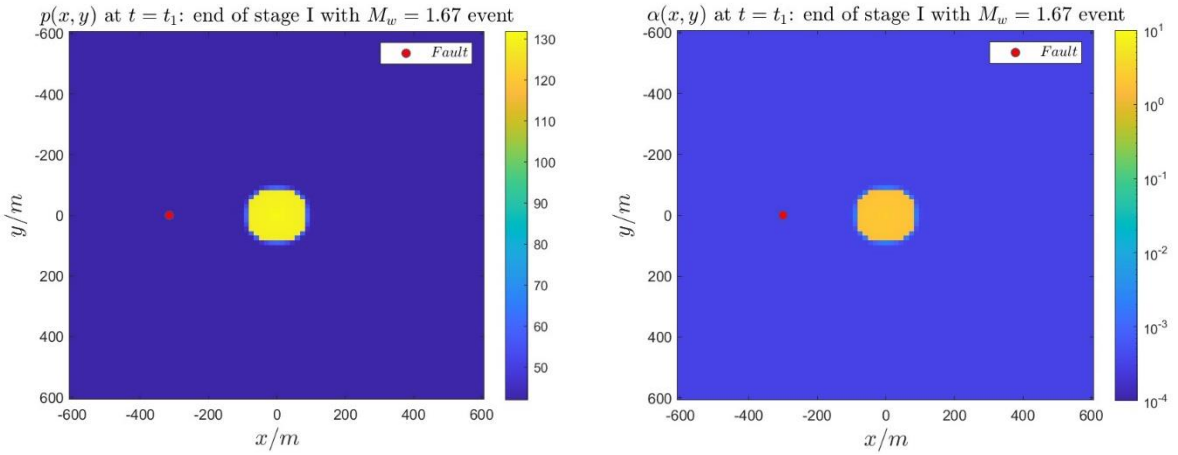

Figure 11: Fluid pressure distribution (left) and hydraulic diffusivity (right) on hydraulic fracture plane at the end of stage I: injection phase.

The hydraulic fracture plane intersecting the PX_2 well is assumed to be the dominant flow pathway connecting the fault and the well with the pressure-dependent hydraulic diffusivity observed in in-situ injection test. This creates a gradient where hydraulic diffusivity decreases with distance from the well. Near the well, diffusivity can increase by up to 1,000 times, ranging between 1 and 10 m²/s, compared to areas where fluid pressure has not yet reached, where diffusivity remains in the range of 10^{-4} and $10^{-3}\ m^2/s$.

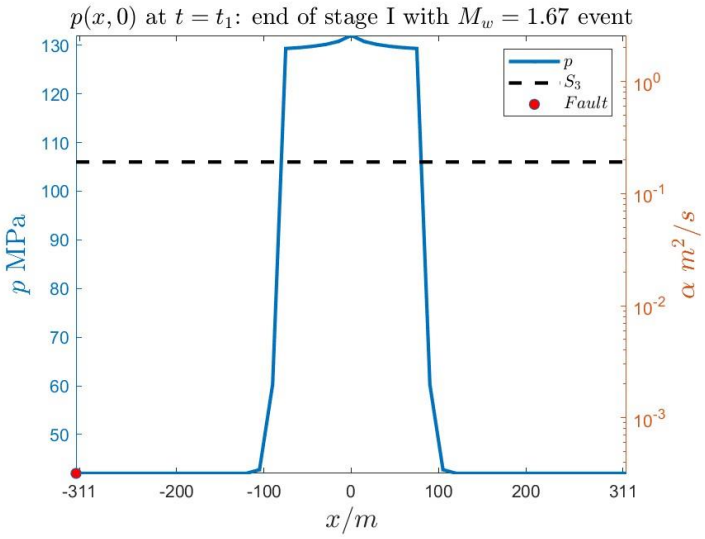

Figure 12: Fluid pressure distribution on a horizontal line between fault and the well at the end of stage I: injection phase.

As shown in Figure 12, in the model the radius of hydraulic opening which is the size of region where net pressure (fluid pressure exceeds the minimum principal stress S_3) is positive is 59.26m. Within this radius, pressure decreases gradually as the spatial pressure gradient is relatively smaller compared to regions farther away, resulting in a steeper pressure front. This behavior can be explained by the conservation of flux, which is the product of permeability k and the pressure gradient $\partial p/\partial x$. For the region away from the well, pressure is lower and induces smaller permeability, leading to a larger pressure gradient and a steeper pressure drop (Murphy et al. 2004). Beyond the steep pressure front, pressure is almost the same as the hydrostatic pressure.

4.1.2 Tensile stress transfer at the end of injection

The radius of hydraulic opening R_{open} is 59.26m and the opening is induced inside the region (Figure 13). Beyond the opening, there is tensile stress transfer. The tensile stress transfer from hydraulic opening goes to infinity at the hydraulic opening tip and gradually decreases away from tip of the hydraulic opening. The tensile stress transfer evaluated at the fault is 0.0477 MPa. For a critically stressed fault, perturbation of stress on fault reach 0.01MPa can induce seismicity (King et al. 1994). Therefore, a tensile stress contribution of 0.0477 MPa represents a significant factor in inducing seismicity.

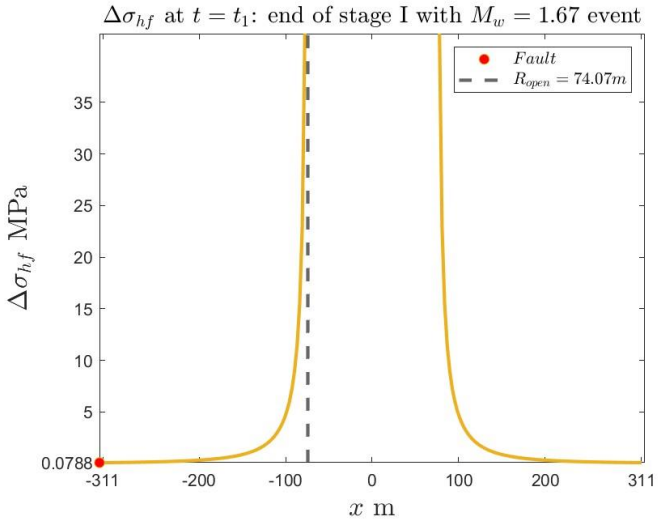

Figure 13: Tensile stress transfer distribution on a horizontal line between fault and the well at the end of stage I: injection phase.

4.2 Stage II: seismically dormant period after injection stopped

During Stage II, the injection stopped and resulted in pressure drop across the fracture (Figure 14). As the pressure dropped below the minimal principal stress, the fracture went from open to closed and deactivated the tensile stress transfer. Meanwhile, the pressure front continued to propagate toward the fault, but its speed was slower due to the reduction in pressure, which in turn decreases hydraulic

diffusivity. The deactivation of both mechanisms likely contributed to decrease of slip on fault, resulting in the observed seismically dormant period.

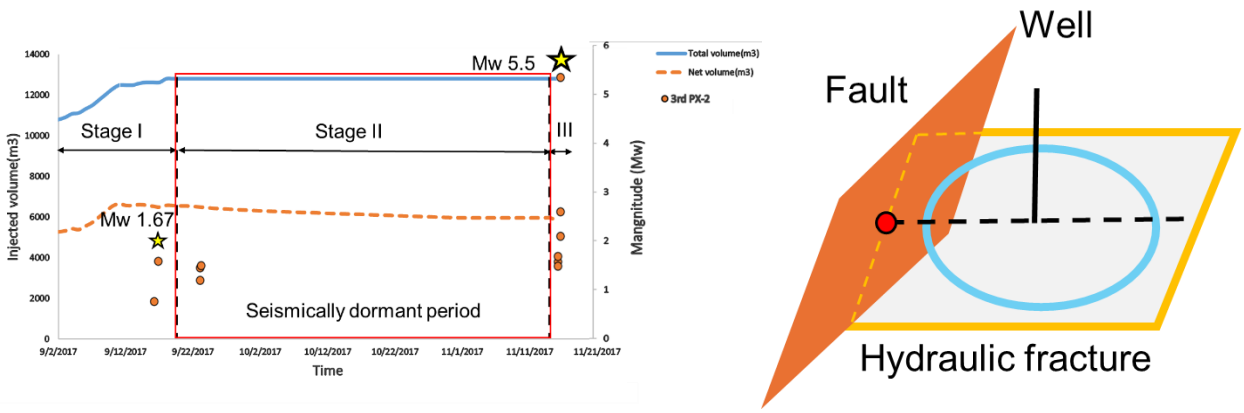

Figure 14: Stage II: a seismically dormant period after injection stopped (left), deactivation of both fluid pressure and tensile stress transfer from hydraulic opening (right)

4.2.1 Pressure distribution after injection stopped

Compared with the fluid pressure and hydraulic diffusivity distribution at the end of stage I in Figure 10, fluid pressure dropped a lot for the region near the injection center and decreased from 132MPa to 68 MPa at the injection center (Figure 15). A decrease in hydraulic diffusivity around the injection center from 1 m^2/s to 10^{-2} m^2/s was observed as well. The region where fluid pressure front reached gets larger.

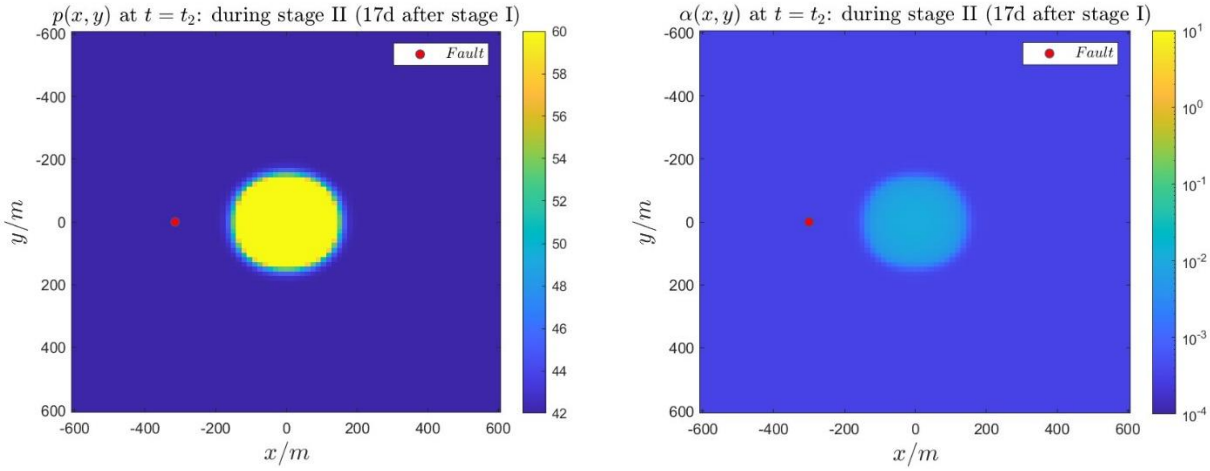

Figure 15: Fluid pressure distribution (left) and hydraulic diffusivity (right) on hydraulic fracture plane during stage I: 17 days after stage I.

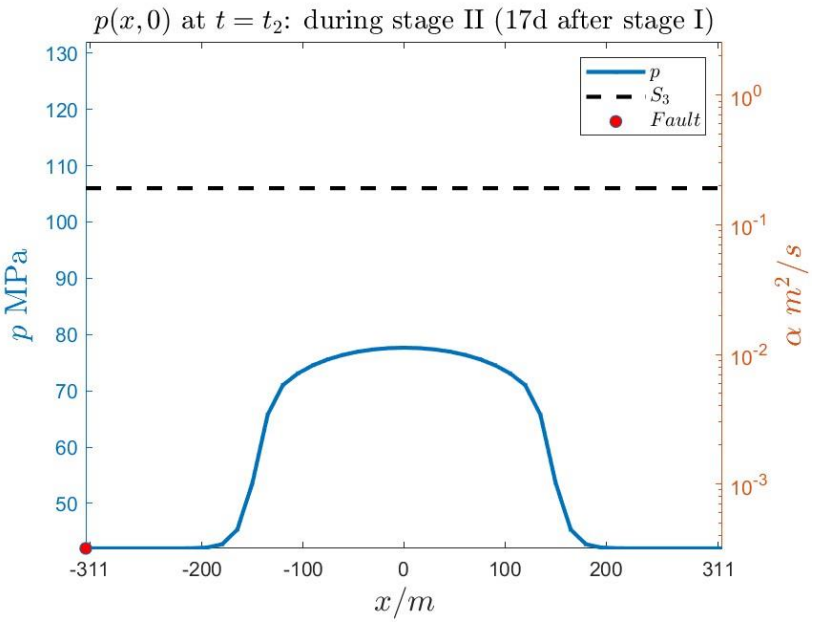

Figure 16: Fluid pressure distribution on the horizontal line connecting fault and well in stage II 17 days after the end of stage I.

Seventeen days after the injection stopped, the pressure fell below the minimum principal stress, causing the fracture to go from open to close (Figure 16). Although the pressure dropped after injection stopped, the pressure front continued propagating but with a slower speed because of the decrease in hydraulic diffusivity. By this point, the front had advanced from around 100 m at the end of Stage I to approximately 200 m.

4.2.2 Tensile stress transfer distribution after injection stopped

After the injection stopped, tensile stress transfer on fault was deactivated because pressure is below the minimal principal stress everywhere and there was no opening (Figure 17). Therefore, both fluid pressure and tensile stress on fault were deactivated and likely contribute to the seismically dormant period.

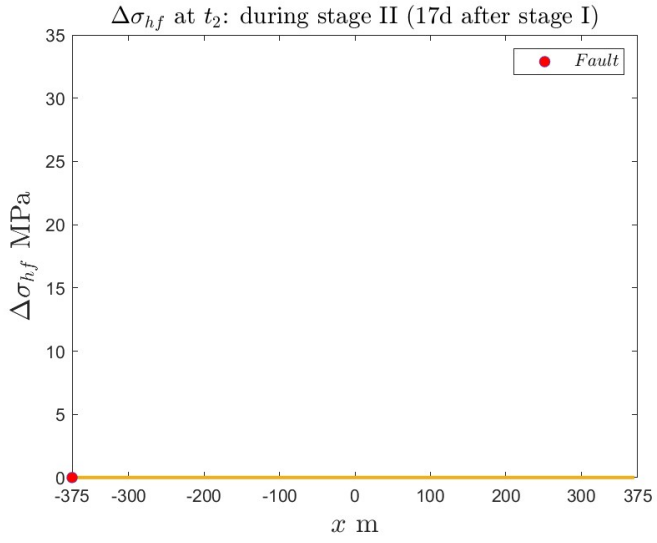

Figure 17: Tensile stress transfer distribution on a horizontal line between fault and the well in stage II 17 days after the end of stage I.

4.3 Stage III: occurrence of Mw 5.5 earthquake

In Stage III, the final Mw 5.5 earthquake occurred with a 58-day delay after the end of Stage I (injection). After sufficient time for propagation, the pressure front reached the fault, resulting in an increase in fluid pressure and perturbing the stress on the fault. The activation of fluid pressure likely contributed to the delayed Mw 5.5 earthquake (Figure 18).

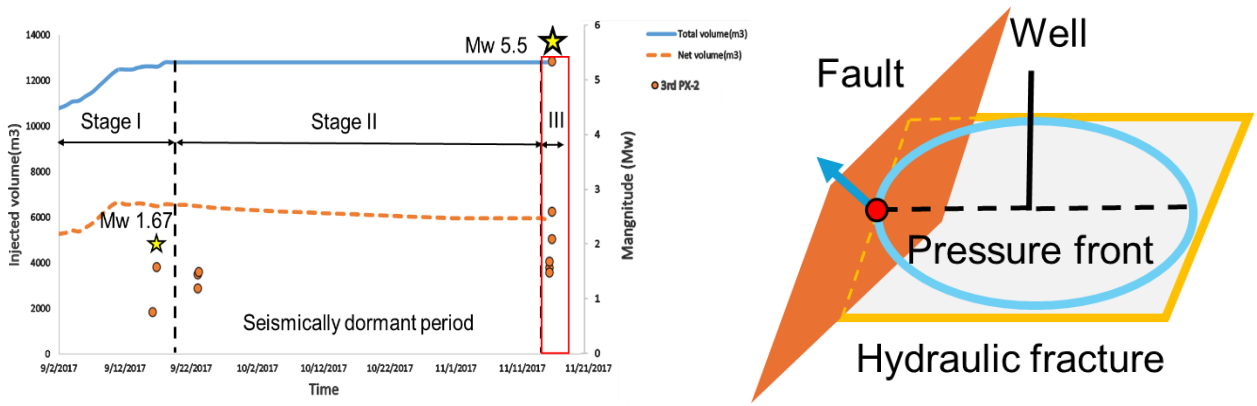

Figure 18: Stage III: occurrence of the Mw 5.5 event (left), deactivation of both fluid pressure and tensile stress transfer from hydraulic opening (right)

4.3.1 Pressure and tensile stress transfer distribution when pressure front reached fault

Compared with the fluid pressure and hydraulic diffusivity distribution at the end of stage II in Figure 10, fluid pressure keeps dropping from stage II and the pressure in the injection center decreased from 68MPa to 55MPa (Figures 19 and 20). Hydraulic diffusivity across the fracture decreased as well.

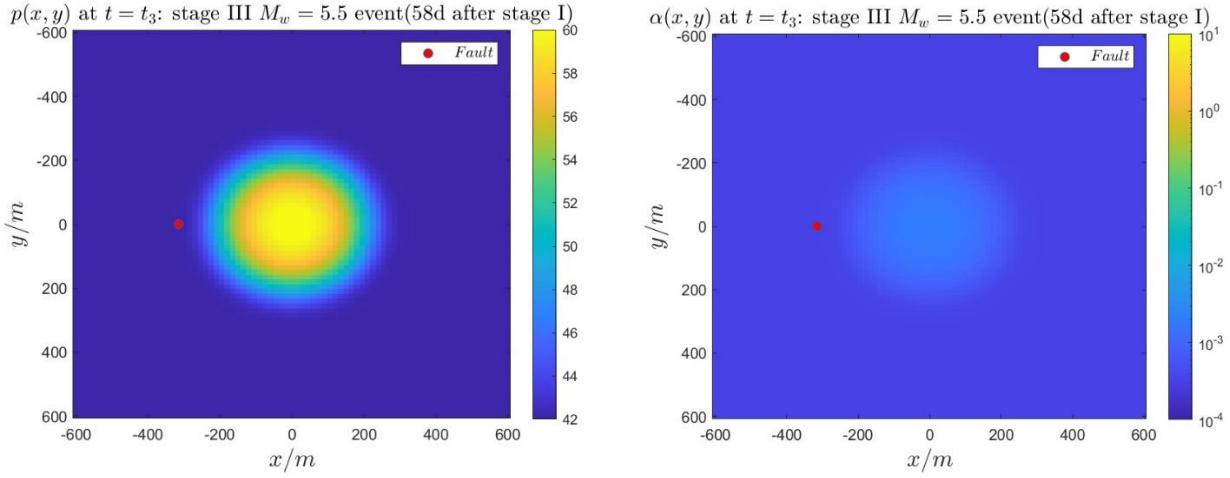

Figure 19: Fluid pressure distribution (left) and tensile stress transfer distribution on the line (right) on hydraulic fracture plane in stage III: 58 days after the end of stage I.

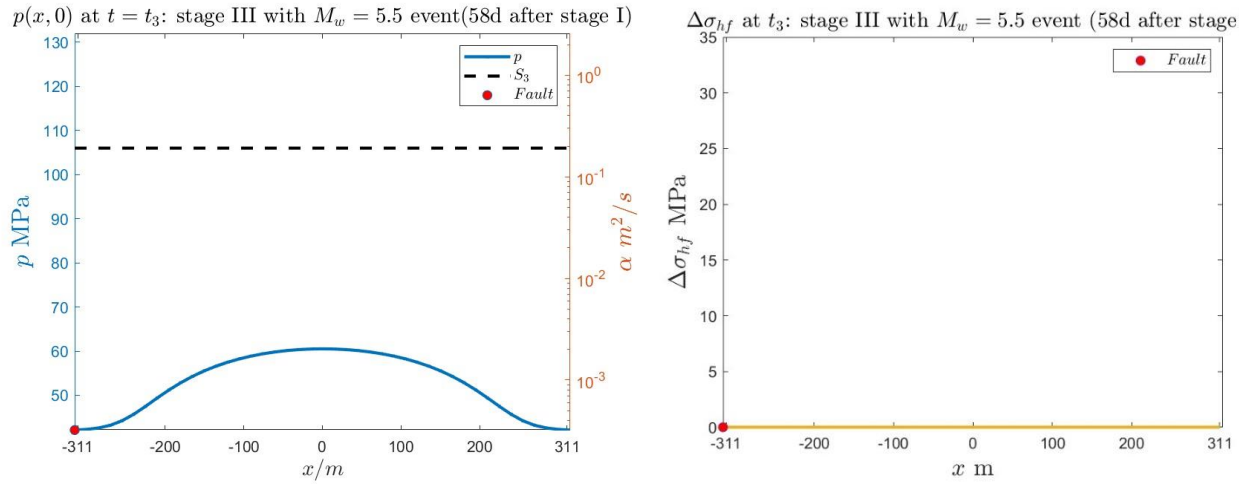

Figure 20: Fluid pressure distribution (left) and hydraulic diffusivity (right) on hydraulic fracture plane in stage III: 58 days after the end of stage I.

As pressure around the injection center continued to drop, the pressure front eventually reached the fault. With pressure at all locations on the fracture still below the minimal principal stress, the fracture remained closed, and there was no tensile stress transfer. As a result, the pressure front arrived at the fault 58 days after the end of stage I (injection), leading to an increase in fluid pressure on the fault. This likely contributed to the delayed Mw 5.5 earthquake.

4.4 Fault slip velocity under perturbed stress history from the two mechanisms

4.4.1 Perturbed stress history on fault: fluid pressure and tensile stress transfer from hydraulic opening

The two mechanisms, fluid pressure and tensile stress transfer from hydraulic opening, were activated at different times and contributed to the distinct stages of the induced seismicity sequence (Figure 21). In the model, tensile stress transfer was activated early in Stage I (injection) when fluid pressure near the injection center exceeded the minimal principal stress. Causing the fracture to open. Once the opening occurred, tensile stress transfer was activated instantaneously and perturb the stress on the fault due to elasticity effect. This tensile stress reached its peak of approximately 0.08 MPa at the moment when injection stopped as the hydraulic opening reached its maximum radius. Meanwhile, the fluid pressure front was still propagating towards the fault and has not yet reached it, indicating its effect on the fault remain negligible. In Stage II (post-injection) after injection stopped, pressure dropped below the minimal principal stress, leading to the fracture closure and deactivating the tensile stress transfer. During this stage, both mechanisms were inactive and resulted in no stress perturbation on the fault, which likely explains the observed seismically-dormant period. Stage III began when the fluid pressure front finally reached the fault, causing a rise in fluid pressure and perturbing the fault stress. Unlike tensile stress transfer, which peaked early and then diminished after fracture closure, fluid pressure increased gradually at first but later accelerated. Fluid pressure reached 0.1 MPa 58 days after injection stopped, which falls within the reported range of 0.05 to 0.25 MPa in previous studies (Ellsworth et al., 2019; Lim et al., 2020; Yeo et al., 2020; Chang et al., 2020). This continuous rise in fluid pressure likely triggered the delayed Mw 5.5 earthquake.

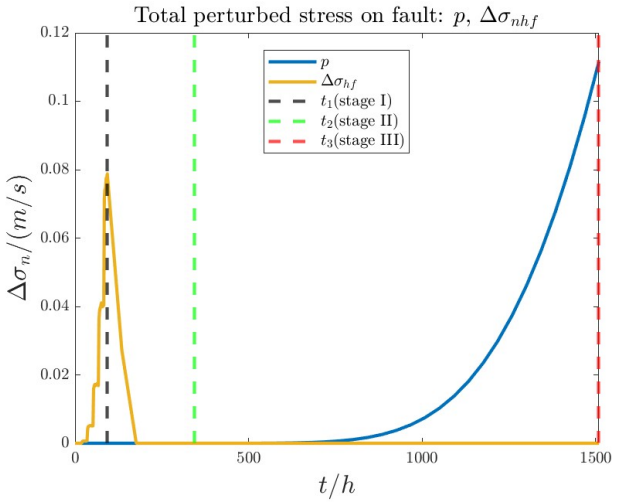

Figure 21: Perturbed stress on fault under two mechanisms: fluid pressure and tensile stress transfer from hydraulic opening.

The perturbed stresses from these two mechanisms exhibit distinct characteristics. Tensile stress transfer was activated earlier, with a rapid increase but a short duration. In contrast, fluid pressure was activated later, increased more gradually at first, then accelerated, ultimately reaching a higher final magnitude. According to the model, the peak tensile stress transfer reached 0.08 MPa, which, despite being lower than the final fluid pressure, is still significant. Given that a critically stressed fault can experience seismic events with stress perturbations as low as 0.01 MPa (King et al. 1994), tensile stress transfer alone could have induced a moderate event. The total perturbed stress, combining contributions from both mechanisms, could provide a possible explanation for the observed induced seismicity sequence.

4.4.2 Fault velocity under the perturbed stress

The slip velocity on the fault was estimated with the spring slider model based on the perturbed stress history, which serves as an indicator of the observed moment magnitude (Figure 22). Fault velocity began to increase as soon as hydraulic opening was initiated during injection and reached its local maximum by the time injection stopped. This increase corresponded to the moderate Mw 1.67 event that occurred around the time when injection stopped, driven by the rising tensile stress transfer associated with the expanding hydraulic opening. After injection stopped, the tensile stress transfer was deactivated due to fracture closure, leading to a reduction in perturbed stress. As a result, the fault velocity slowed down and returned to its reference value, corresponding to the seismically-dormant period. However, once the pressure front reached the fault, fluid pressure began to increase again and reactivated fault slip. Initially when the pressure front arrived, both pressure increases were gradual, leading to only a minor rise in fault velocity. Overtime, as fluid pressure continued to build and its

rate of increase accelerated, the slip velocity surged marking the transition from interseismic to the coseismic phase and ultimately providing conditions that could have triggered the delayed Mw 5.5 earthquake.

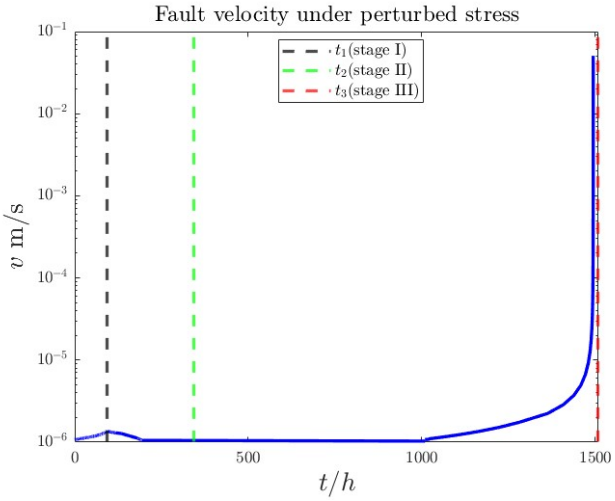

Figure 22: Evolution of slip velocity on fault under perturbed stress.

4.4 Sensitivity analysis of hydraulic diffusivity and its implication on seismic event magnitude and timing

Hydraulic diffusivity is one of the most uncertain parameters in the flow model, with reported values ranging from $10^{-4} - 10\ m^2/s$ over approximately five orders of magnitude in Pohang (Lim et al. 2020, Kim et al. 2022, Chang et al. 2020, Ellsworth et al. 2019). This parameter significantly influences the pressure evolution and, consequently, the activation, timing, and intensity of the two proposed mechanisms, affecting seismic event magnitude and occurrence. Field measurements, including in-situ tests from Pohang, have demonstrated that hydraulic diffusivity in fractures is stress-sensitive and follows an exponential relationship with pressure (Park et al. 2017). This relationship is characterized by two key parameters: the initial hydraulic diffusivity and the enhancement rate with pressure (Park et al. 2020, Kim et al. 2022). We investigate the sensitivity of the two parameters concerning (1) the maximum tensile stress transfer at the time of injection stoppage and (2) the arrival time of the pressure front at the fault. These factors correspond to the seismic event triggered at the end of injection in Stage I and the delayed Mw 5.5 earthquake in Stage III, respectively.

4.4.1 Sensitivity to initial hydraulic diffusivity

To examine the influence of initial hydraulic diffusivity on seismic event magnitude and timing, we tested seven different initial hydraulic diffusivity values and compared them to the reference case (($\overline{\alpha_0}$), which corresponds to the observed 58-day delay. Figure 23 (left) illustrates the evolution of hydraulic diffusivity with pressure for three representative values which are low, equal, and high relative to ($\overline{\alpha_0}$). Figure 23 (right) presents the corresponding perturbed stress on the fault.

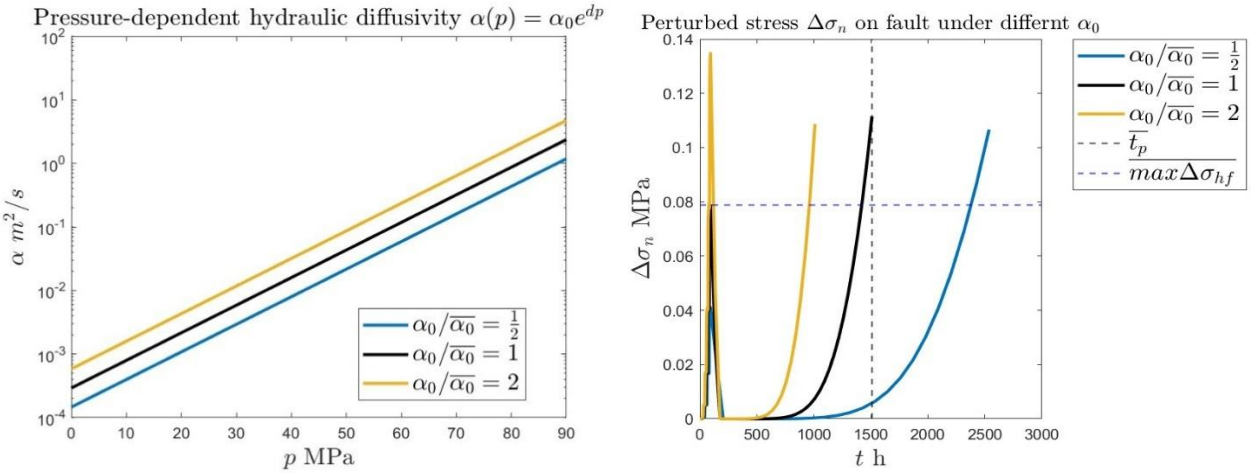

Figure 23: Change of hydraulic diffusivity with pressure (left), and perturbed stress history under different initial hydraulic diffusivity (right) under different initial hydraulic diffusivity.

The results show that lower initial hydraulic diffusivity delays the pressure front arrival and reduces the maximum tensile stress transfer. This occurs because lower diffusivity slows both the propagation of the pressure front and the growth of hydraulic opening. Conversely, higher initial hydraulic diffusivity results in a faster pressure front arrival and increased tensile stress transfer. When injection stops, the maximum tensile stress transfer can exceed 0.1MPa, comparable to the final fluid pressure level in the reference case. This suggests that under high hydraulic diffusivity, the fault may experience stress perturbations strong enough to induce seismic events during injection rather than post-injection.

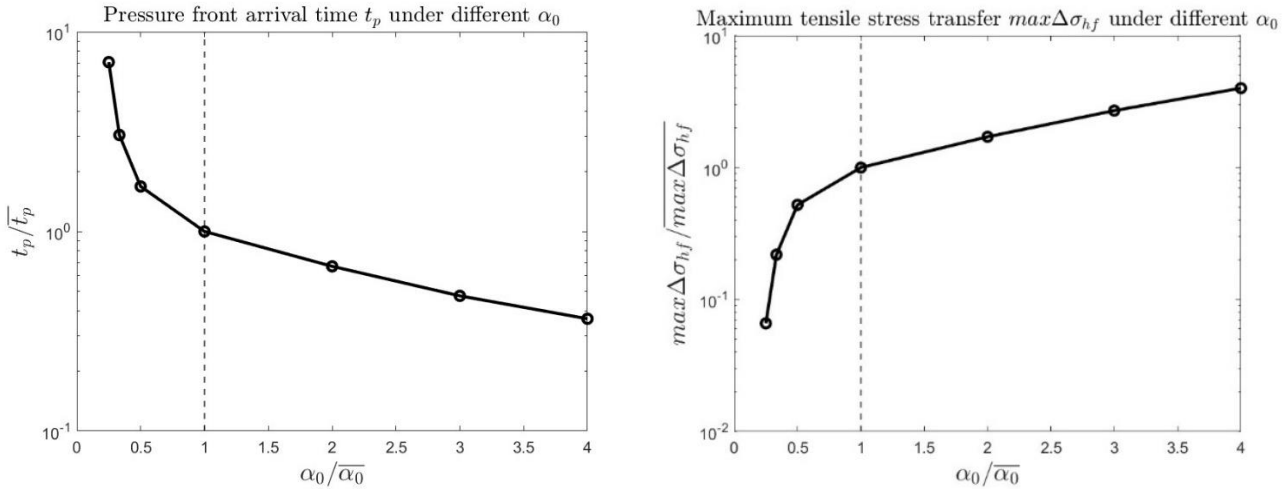

Figure 24: Normalized pressure front arrival time (left) and normalized maximal tensile stress transfer when injection stopped (right) under different initial hydraulic diffusivity.

Figure 24 shows how sensitive the pressure front arrival time and maximal tensile stress transfer are with the change in initial hydraulic diffusivity. When initial hydraulic diffusivity is low as $\alpha_0/\bar{\alpha}_0 < 1$, both the arrival time and the tensile stress transfer are more sensitive to the change with initial hydraulic diffusivity. It may indicate the importance of constraining hydraulic diffusivity range and overestimate hydraulic diffusivity in practice may be a safer choice for operation.

4.4.2 Sensitivity to hydraulic diffusivity enhancement rate

The hydraulic diffusivity enhancement rate determines how rapidly hydraulic diffusivity increases with pressure, which refers to the slope in Figure 25 (right). A higher enhancement rate leads to an increase in the maximum principal stress and an earlier arrival of the pressure front. Compared to the effect of increasing initial hydraulic diffusivity (Figure 23), a higher enhancement rate also results in faster pressure buildup after the pressure front reaches the fault. This occurs because a higher permeability enhancement rate results in stronger spatially heterogeneous hydraulic diffusivity and leads to a steeper pressure front.

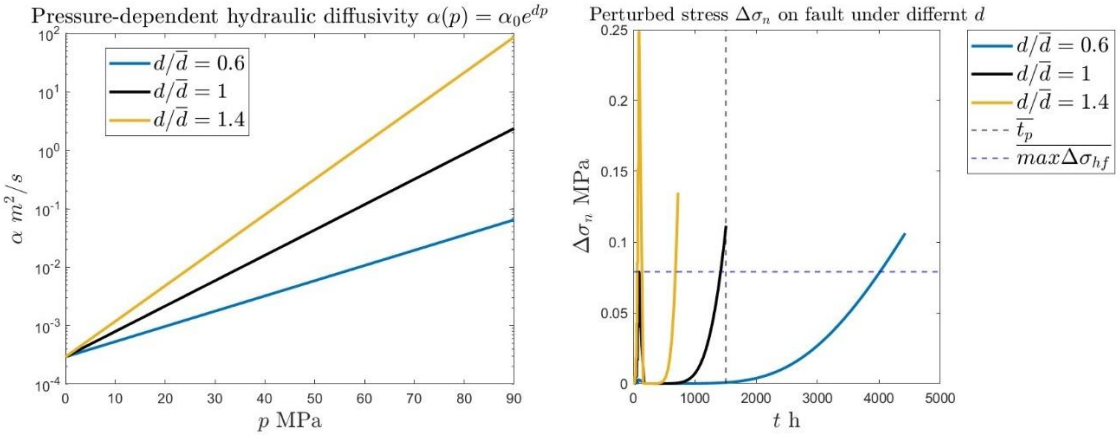

Figure 25: Change of hydraulic diffusivity with pressure (left), and perturbed stress history under different initial hydraulic diffusivity (right) under different hydraulic diffusivity enhancement rates.

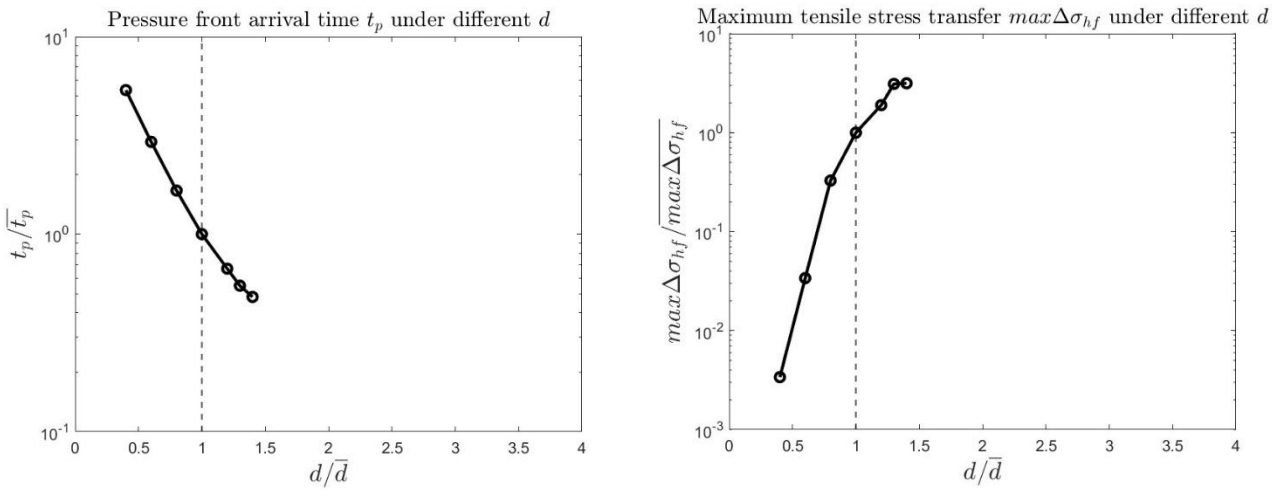

Figure 26: Normalized pressure front arrival time (left) and normalized maximal tensile stress transfer when injection stopped (right) under different hydraulic diffusivity enhancement rates.

Unlike the broad range of initial hydraulic diffusivity values (Figure 24), the enhancement rate is constrained to ensure the resulting hydraulic diffusivity remains within a reasonable range (10^{-4} -100 m^2/s). This constraint limits the enhancement rate to approximately be smaller than 1.4. Similar to the effects of initial hydraulic diffusivity, a higher permeability enhancement rate under a fixed initial hydraulic diffusivity result in a shorter pressure front arrival time and a larger maximum tensile stress transfer due to the overall increase in hydraulic diffusivity (Figure 26). However, unlike initial hydraulic diffusivity, the sensitivity of pressure front arrival time and tensile stress transfer remains relatively consistent across different enhancement rates (Figure 26).

These findings have four implications for seismic hazard assessment: (1) Large earthquake during injection: Higher hydraulic diffusivity leads to greater tensile stress transfer, which may induce a significant earthquake during injection rather than after injection stops. (2) A single delayed earthquake under low diffusivity: When hydraulic diffusivity is low, tensile stress transfer remains weak, potentially not enough to cause seismic events during injection. However, a delayed earthquake can still occur in post-injection, possibly reaching a higher magnitude due to sustained fluid pressure buildup. (3) Importance of constraining hydraulic diffusivity and permeability enhancement rate: Microseismicity data from hydraulic fracturing can help estimate hydraulic diffusivity values. Besides, injection tests can be used to characterize permeability changes under different pressures. (4) Overestimating hydraulic diffusivity as a conservative approach in seismicity hazard mitigation: Higher estimated hydraulic diffusivity accounts for greater tensile stress transfer and earlier pressure front arrival, which makes it a safer approach for mitigating seismic hazard.

5. CONCLUSION

In this study, we investigated mechanisms beyond fluid pressure increase by combining tensile stress transfer from hydraulic opening to explain the induced seismicity sequence observed in the Pohang EGS project. Our findings show that these two mechanisms would be activated at different times with different intensities, which would contribute to distinct stages of the seismicity sequence. In the model, tensile stress transfer was activated instantaneously when the hydraulic fractures opened during injection due to elasticity. Its magnitude is relatively low and duration is relatively short, which may contribute to the moderate Mw 1.67 event at the time around injection stopped. At this point, fluid pressure had not yet reached due to its finite propagation speed and remained inactive. After injection stopped, fracture closure led to the deactivation of both mechanisms, which may contribute to the seismically dormant period observed in post-injection. Once the pressure front eventually reached the fault, a continuous pressure increase may resume seismicity. This pressure buildup over time exceeded the peak magnitude of the earlier tensile stress transfer, which could serve as a trigger for the delayed Mw 5.5 earthquake 58 days after injection stopped.

REFERENCES

Alcolea, A., Meier, P., Vilarrasa, V., Olivella, S., and Carrera, J.: Hydromechanical modeling of the hydraulic stimulations in borehole PX2 (Pohang, South Korea), Geothermics, 120, (2024).

Boyet, A., de Simone, S., Ge, S., and Vilarrasa, V. Poroelastic stress relaxation, slip stress transfer and friction weakening controlled post-injection seismicity at the Basel Enhanced Geothermal System, Communications Earth and Environment, 4, (2023).

Catalli, F., Meier, MA., and Wiemer, S.: The role of Coulomb stress changes for injection-induced seismicity: the Basel enhanced geothermal system, Geophysical Research Letters, 40, (2013), 72–77.

Chang, KW., and Segall P.: Injection-induced seismicity on basement faults including poroelastic stressing: Journal of Geophysical Research Solid Earth, 121(4), (2016), 2708–2726.

Cuenot, N., Dorbath, C., and Dorbath, L.: Analysis of the microseismicity induced by fluid injections at the EGS site of Soultz-sous-Forêts (Alsace, France): Implications for the characterization of the geothermal reservoir properties. Pure and Applied Geophysics, 165, (2008), 797-828.

Dieterich, J. H.: Modeling of rock friction 1. Experimental results and constitutive equations, Journal of Geophysical Ressearch Solid Earth, 84, (1979), 2161–2168.

Ellsworth, W. L., Giardini, D., Townend, J., Ge, S., and Shimamoto, T.: Triggering of the Pohang, Korea, Earthquake (Mw 5.5) by enhanced geothermal system stimulation, Seismological Research Letters, 90, (2019), 1844–1858.

Häring, M. O., Schanz, U., Ladner, F., and Dyer, B. C.: Characterisation of the Basel 1 enhanced geothermal system, Geothermics, 37, (2019), 469–495.

Kettlety, T., Verdon, J.P., Werner, M.J., Kendall, J.M., and Budge, J.: Investigating the role of elastostatic stress transfer during hydraulic fracturing-induced fault activation, Geophysical Journal International, 217, (2019), 1200–1216.

King, G. C. P., Stein, R. S. and Lin, J: Static stress changes and the triggering of earthquakes. Bulletin of the Seismological Society of the America, 84, (1994), 935–953.

Kivi, I. R., Boyet, A., Wu, H., Walter, L., Hanson-Hedgecock, S., Parisio, F., and Vilarrasa, V.: Global physics-based database of injection-induced seismicity, Earth System Science Data, 15, (2023), 3163–3182.

Kim, K. il, Yoo, H., Park, S., Yim, J., Xie, L., Min, K. B., and Rutqvist, J.: Induced and triggered seismicity by immediate stress transfer and delayed fluid migration in a fractured geothermal reservoir at Pohang, South Korea, International Journal of Rock Mechanics and Mining Sciences, 153, (2022).

Korean Government Commission (KGC): Final Report of the Korean Government Commission on Relations between the 2017 Pohang Earthquake and EGS Project, Geological Society of Korea, (2019).

Lim, H., Deng, K., Kim, Y.H.: The 2017 Mw 5.5 Pohang earthquake, South Korea, and poroelastic stress changes associated with fluid injection, Journal of Geophysical Research Solid Earth, 124, (2020), 1–18.

Min K. B., Rutqvist, J., Tsang, C. F., and Jing, L.: Stress-dependent permeability of fractured rock masses: A numerical study. International Journal of Rock Mechanics and Mining Sciences, 41, (2004), 1191–1210.

Min K. B., Park, S., Kim, K. il, Yoo, H., Kwon, S., Yim, J. and Rutqvist, J., Enhancement of Steam Phase Relative Permeability Due to Phase Transformation Effects in Porous Media, Proceedings, 48th Workshop on Geothermal Reservoir Engineering, Stanford University, Stanford, CA (2023).

McClure, M. W., and Horne, R. N.: Investigation of injection-induced seismicity using a coupled fluid flow and rate/state friction model. Geophysics, 76, (2011).

Murphy, H., Huang, C., Dash, Z., Zyvoloski, G., and White, A.: Semianalytical solutions for fluid flow in rock joints with pressure-dependent openings, Water Resources Research, 40, (2004), 1–16.

Noda, H., Dunham, E. M., and Rice, J. R.: Earthquake ruptures with thermal weakening and the operation of major faults at low overall stress levels. Journal of Geophysical Research: Solid Earth, 114, (2009).

Ozawa, S., Ida, A., Hoshino, T., & Ando, R.: Large-scale earthquake sequence simulations on 3-D non-planar faults using the boundary element method accelerated by lattice H-matrices, Geophysical Journal International, 232, (2023), 1471–1481.

Park, S., Xie, L., Kim, K. il, Kwon, S., Min, K. B., Choi, J., Yoon, W. S., and Song, Y.: First Hydraulic Stimulation in Fractured Geothermal Reservoir in Pohang PX-2 Well, Procedia Engineering, 191, (2017), 829–837.

Park, S., Kim, K. il, Xie, L., Yoo, H., Min, K. B., Kim, M., Yoon, B., Kim, K. Y., Zimmermann, G., Guinot, F., & Meier, P. (2020). Observations and analyses of the first two hydraulic stimulations in the Pohang geothermal development site, South Korea, Geothermics, 88, (2020).

Rutqvist, J., Stephansson, O.: A cyclic hydraulic jacking test to determine the in-situ stress normal to a fracture. International Journal of Rock Mechanics and Mining Sciences, 33, (1996), 695–711.

Rutqvist, J., and Tsang, C. F.: Analysis of thermal-hydrologic-mechanical behavior near an emplacement drift at Yucca Mountain. Journal of Contaminant Hydrology, 62–63, (2003), 637–652.

Woo, J. U., Kim, M., Sheen, D. H., Kang, T. S., Rhie, J., Grigoli, F., Ellsworth, W. L., and Giardini, D.: An In-Depth Seismological Analysis Revealing a Causal Link Between the 2017 MW 5.5 Pohang Earthquake and EGS Project, Journal of Geophysical Research: Solid Earth, 124, (2019), 13060–13078.

Wong, L. N. Y., and Cui, X.: DDFS3D: A set of open-source codes leveraging hybrid 3D displacement discontinuity method and fictitious stress method to simulate fractures, Engineering Analysis with Boundary Elements, 131, (2021), 146–158.

Yeo, I.W., Brown, M.R.M., Ge, S. and Lee, K.K.: Causal mechanism of injection-induced earthquakes through the Mw 5.5 Pohang earthquake case study, Nature Communication, 11, 2020, 2614.